ARMY RESEARCH LABORATORY

Through-Thickness Property Measurement of Three-Dimensional Textile Composites

by Ryan L. Karkkainen, Paul Moy, and Jerome T. Tzeng

ARL-TR-4765 **April 2009**

NOTICES

Disclaimers

Army Research Laboratory
Aberdeen Proving Ground, MD 21005-5069

ARL-TR-4765 **April 2009**

Through-Thickness Property Measurement of Three-Dimensional Textile Composites

Ryan L. Karkkainen
The Oak Ridge Institute for Science and Education

Paul Moy and Jerome T. Tzeng
Weapons and Materials Research Directorate, ARL

REPORT DOCUMENTATION PAGE						*Form Approved* *OMB No. 0704-0188*
Public reporting burden for this collection of information is estimated to average 1 hour per response, including the time for reviewing instructions, searching existing data sources, gathering and maintaining the data needed, and completing and reviewing the collection information. Send comments regarding this burden estimate or any other aspect of this collection of information, including suggestions for reducing the burden, to Department of Defense, Washington Headquarters Services, Directorate for Information Operations and Reports (0704-0188), 1215 Jefferson Davis Highway, Suite 1204, Arlington, VA 22202-4302. Respondents should be aware that notwithstanding any other provision of law, no person shall be subject to any penalty for failing to comply with a collection of information if it does not display a currently valid OMB control number. **PLEASE DO NOT RETURN YOUR FORM TO THE ABOVE ADDRESS.**						
1. REPORT DATE *(DD-MM-YYYY)* April 2009		**2. REPORT TYPE** Final				**3. DATES COVERED (From - To)** October 2006–September 2008
4. TITLE AND SUBTITLE Through-Thickness Property Measurement of Three-Dimensional Textile Composites						**5a. CONTRACT NUMBER**
						5b. GRANT NUMBER
						5c. PROGRAM ELEMENT NUMBER
6. AUTHOR(S) Ryan L. Karkkainen,* Paul Moy, and Jerome T. Tzeng						**5d. PROJECT NUMBER** 622618H80
						5e. TASK NUMBER
						5f. WORK UNIT NUMBER
7. PERFORMING ORGANIZATION NAME(S) AND ADDRESS(ES) U.S. Army Research Laboratory ATTN: AMSRD-ARL-WM-MB Aberdeen Proving Ground, MD 21005-5069						**8. PERFORMING ORGANIZATION REPORT NUMBER** ARL-TR-4765
9. SPONSORING/MONITORING AGENCY NAME(S) AND ADDRESS(ES)						**10. SPONSOR/MONITOR'S ACRONYM(S)**
						11. SPONSOR/MONITOR'S REPORT NUMBER(S)
12. DISTRIBUTION/AVAILABILITY STATEMENT Approved for public release; distribution is unlimited.						
13. SUPPLEMENTARY NOTES *The Oak Ridge Institute for Science and Education, 4692 Millenium Dr., Ste. 101, Belcamp, MD 21017						
14. ABSTRACT Three-dimensional (3-D) reinforcement of thick composite parts is utilized to increase delamination resistance and through-thickness properties, which often represent the weak link of such structures. Stitching, z-pinning, or a 3-D textile weave may be employed. In the current study of a 3-D, orthogonal-woven, glass-epoxy composite, a specimen is designed for cases in which a sufficiently thick specimen for standard test setups cannot be created due to manufacturing limitations. A minimum width is dictated by the need to capture a sufficient number of through-thickness stitches in the specimen cross section. Thickness is limited by manufacturing feasibility, as stitches can only penetrate through a certain thickness, and further limitation is imposed by the ability of resin to penetrate the fiber preform during cure. Thus, a specimen must accommodate this low aspect ratio geometry. To this end, several specimens have been designed using finite-element method analysis and validated experimentally. Multiple specimen types were investigated to determine an optimum specimen and to ensure geometry independence of the obtained properties. Optimized specimens have shown good agreement with stiffness predictions as well as promising, consistent results for strength determination.						
15. SUBJECT TERMS composites, textile reinforcement, 3-D woven, strength						
16. SECURITY CLASSIFICATION OF:			**17. LIMITATION OF ABSTRACT**		**18. NUMBER OF PAGES**	**19a. NAME OF RESPONSIBLE PERSON** Ryan Karkkainen
a. REPORT Unclassified	**b. ABSTRACT** Unclassified	**c. THIS PAGE** Unclassified	UU		22	**19b. TELEPHONE NUMBER** *(Include area code)* 410-306-0710

Standard Form 298 (Rev. 8/98)
Prescribed by ANSI Std. Z39.18

Contents

List of Figures

List of Tables

Acknowledgments

This project was supported in part by the Research Participation Program for the U.S. Army Research Laboratory (ARL) administered by the Oak Ridge Institute for Science and Education through an agreement between the U.S. Department of Energy and ARL. The authors would like to express their appreciation to Drs. Shridhar Yarlagadda and John (Jack) Gillespie for their efforts in three-dimensional composite manufacturing under the sponsorship of the Army Composites Materials Technology program.

INTENTIONALLY LEFT BLANK.

1. Introduction

The three-dimensional (3-D) orthogonal weave and other 3-D textile reinforcements are often used in thick composite parts to increase delamination resistance and through-thickness properties. The 3-D orthogonal weave incorporates fiber tows directly in the through-thickness direction. This is of critical importance to delamination resistance, an otherwise common weak point of thick composite structures. Such fiber architectures offer potential structural improvements for applications involving impact, multidimensional loading, or thick sections with relatively large through-thickness or interlaminar shear stresses. Thus they are currently targeted for evaluation as candidate materials for the insulator section of an electromagnetic railgun barrel. When describing the properties directly related to delamination resistance, it is useful to obtain through-thickness stiffness and strength properties. This knowledge also feeds directly into material models yielding improved capabilities for strength prediction of the unique through-thickness failure modes.

Given the microstructural complexity, 3-D woven composites exhibit multiple potential failure mechanisms (*1*), which depend upon the loading conditions and particulars of the layup and constituent materials. The 3-D weaves consistently show improved damage resistance over their two-dimensional counterparts, owing to the energy-absorbing capacity enhanced by the *z*-direction fiber tows (*2*, *3*). The 3-D weaves also show more capacity to absorb multiple strikes before perforation and show less damage localization (*4*). In addition to improved impact performance, the effects of *z*-stitching upon shear properties have been shown experimentally, with increased delamination resistance and significantly increased compression-after-impact capacity (*5*, *6*).

Finite-element method (FEM)-based micromechanical methods for strength modeling of textile composites have been explored in previous works by Karkkainen and coworkers (*7–9*). Improved micromechanical techniques were applied to develop failure envelopes and a quadratic stress gradient failure theory for a plain-weave textile composite. Applying these methods to successful failure prediction for 3-D orthogonal composites has been recently accomplished, yet key experimentally determined information about through-thickness properties and failure modes is needed for further model development and verification.

Excellent treatment of direct measurement of through-thickness properties of laminated composites has been given in Schubel et al. (*10*). Through-thickness off-axis failure envelopes are developed and compared with several failure theories and a proposed new approach to predicting this failure regime. Existing techniques for measuring through-thickness properties (*11*, *12*) are generally not developed for directly measuring properties for textile architectures with through-thickness reinforcement. Several relatively new, specialized specimens have been developed to address through-thickness testing of polymer matrix composites (*13–15*) but again are not developed for those including translaminar or through-thickness reinforcement.

The current work involves developing a specimen designed to allow direct measurement of through-thickness properties of a 3-D orthogonal composite. Though there are several difficulties in obtaining a direct measurement of through-thickness stiffness and strength, doing so can provide the valuable advantage of assuring a true property, as well as exhibiting the true failure mode for through-thickness loading. Difficulties in direct measurements for the 3-D orthogonal architecture, which incorporates through-thickness reinforcement, arise for several reasons. First, a standard test specimen (such as ASTM E-8 or D-638 or ISO 527-5) cannot be used for this weave architecture for a specimen aligned in the through-thickness direction. This is due to the fact that such a geometry requires a long specimen to meet the needed aspect ratio. However, the total possible thickness for such an architecture is quite limited by restrictions on the possible thickness of the preform. Further, multiple-stacked preforms are not suitable, as this would introduce nonrepresentative discontinuities between preforms and issues with regards to the quality and uniformity of resin infusion toward the center of the part. Additionally, a through-thickness specimen must capture many through-thickness tows in order to be representative of the continuum properties of the material. Due to the spacing of these through-thickness tows, severe limitations are placed on the minimum thickness. Given all of these complicating factors, a specimen of fairly low ("squat") aspect ratio is required. This in turn gives rise to certain problems. Some amount of taper will be required in order for the bond strength or attachment strength to be greater than the actual through-thickness strength of the specimen. Any taper to the specimen then complicates the stress profile, which should be uniform in the ideal specimen. All of these considerations must be balanced when designing a proper through-thickness test specimen. No current standardized specimen exists that is adequate to this criterion. Several specimen geometries have been evaluated using FEM analysis. Promising candidates were then experimentally tested to evaluate their potential.

2. Finite-Element Modeling for Specimen Evaluation

Figure 1 shows a representative volume element of the 3-D orthogonal weave under investigation. The constituent materials are S2 glass fibers strung in bundles or tows in a 5250-4 bismaleimide (BMI) resin matrix. In figure 1, "warp" tows represent fiber bundles that are aligned in the *x*-axis direction. "Weft" tows are those aligned in the direction of the *y*-axis, and "stitches" are aligned in the *z*-axis or through-thickness direction.

In-plane stiffness properties shown in table 1 are known from previous experimental testing, while through-thickness stiffness is predicted from micromechanical modeling. Given the complexities of the 3-D orthogonal architecture, through-thickness strength prediction is difficult

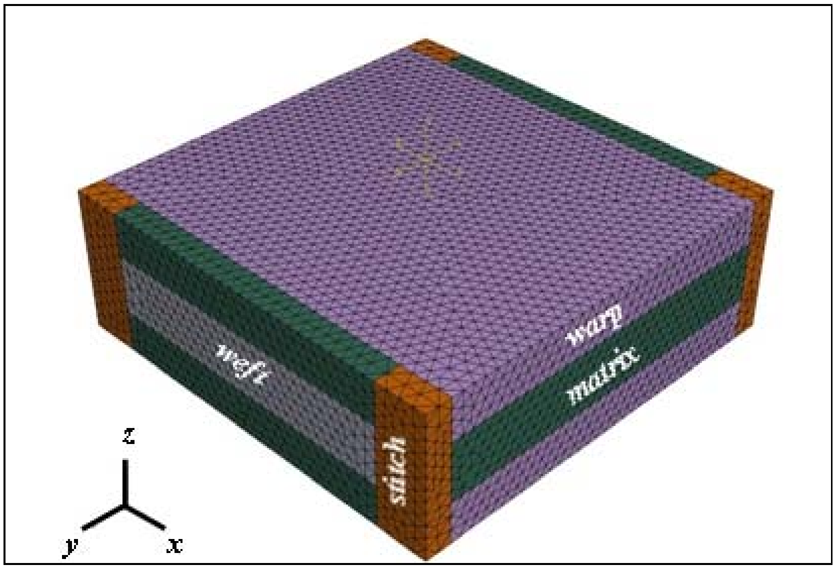

Figure 1. Representative volume element of the 3-D orthogonal weave under investigation.

Table 1. The 3-D orthogonal weave stiffness properties used in modeling (Pa).

Property	Description	Value
E_X	x-axis stiffness (experimental)	2.25 e10
E_Y	y-axis stiffness (experimental)	2.26 e10
E_Z	z-axis stiffness (predicted)	9.28 e9

to achieve without some experimental preknowledge of the failure modes. Properties are homogenized in that individual stitches, fiber tows, etc., are not discretely modeled.

Several specimen types are chosen as starting points for design iterations. For simplicity, a simple tapered cylinder specimen is one of the chosen geometries. Two other candidates are based upon adaptations of the Royal Armament Research and Development Establishment (RARDE) specimen and the circular-waisted block (CWB) (*12–15*). These base geometries, which have been iterated upon, are shown in figure 2a–c. Note that in actuality, each specimen has some "shoulder" material not shown in the schematics. Modeling was performed with the following objectives: (1) ensure an adequately uniform stress distribution at the gage section to yield accurate results, (2) ensure avoidance of excessive stress concentration factor due to edges, corners, or tapers, and (3) provide an estimation of the specimen gage-section failure strength (which must be lower in comparison to the specimen shoulder strength, or the strength of any bonding or fixturing between the specimen and test apparatus). Specimens are modeled using the Abaqus finite-element analysis package. Approximately 35,000 tetrahedral elements are employed per specimen in a static-general analysis. A small z-direction extension is applied to the top boundary of each specimen while the bottom boundary is fixed. Results are then evaluated as per the three aforementioned objectives, and where necessary, the specimen geometry is altered and reevaluated.

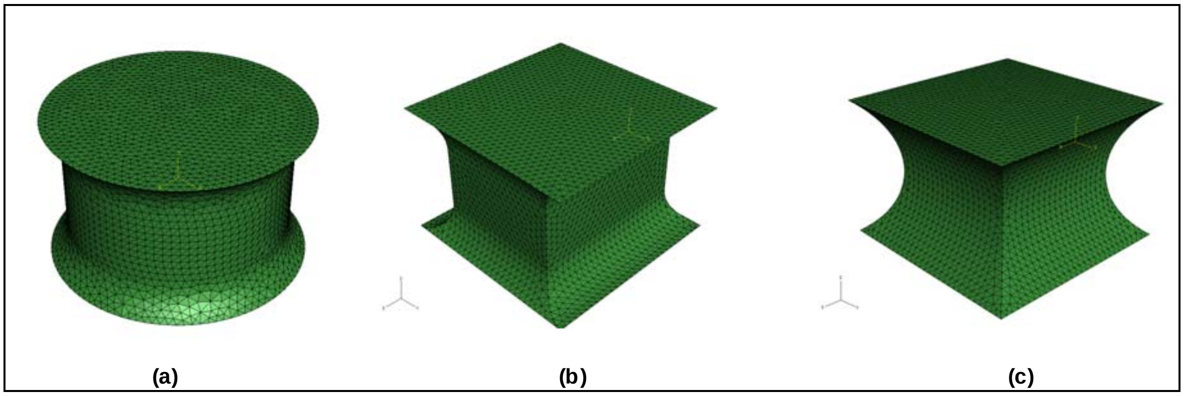

Figure 2. Schematics of the test specimen types: (a) tapered cylinder, (b) RARDE, and (c) circular-waisted block.

3. Modeling Results and Selection of Experimental Specimens

The height of each specimen is maintained as the maximum allowable due to the previously mentioned manufacturing considerations. A minimum width (which varies depending on the specimen shape) is determined by the need to capture a minimum number of stitches, which are spaced at 1.5 stitches/cm. This ensures that a continuum property is obtained, as opposed to properties that will be overstiff (or overcompliant) if observed in small regions close to a fiber stitch (or matrix pocket). Although this is not an issue with the material-homogenized model, the specimen design must account for this potential experimental issue. Table 2 presents a summary of the results for the initial and final iterations for each specimen type. This illustrates the status quo for each specimen and the best performance that could be redesigned and extracted from each. Stress concentration is reported as a ratio of the maximum to minimum stresses occurring nominally within the gage area. Table 3 presents a summary of the geometry of the initial and final specimen geometries. As seen in figure 3, thickness represents the height of each specimen, which is fixed at the manufacturing limit. Width shows the dimension of the top and bottom of the specimen. Neck represents the minimum dimensions of the tapered-down gage area. Taper radius is the radius of curvature of the taper applied to each specimen.

Table 2. Summary of modeling results for specimen design and selection.

Geometry	**Tapered Cylinder**	**RARDE**	**CWB**
Stress concentration (initial)	1.0	1.23	1.16
Stress concentration (final)	1.0	1.17	1.09

Table 3. Summary of specimen geometry iterations.

Geometry	Thickness (mm)	Width (mm)	Neck (mm)	Taper Radius (mm)
Tapered cylinder (initial)	20	35 (diameter)	30 (diameter)	6
Tapered cylinder (final)	20	35	30	6
RARDE (initial)	20	30 × 30	25 × 20	5
RARDE (final)	20	30 × 30	25 × 25	6
CWB (initial)	20	30 × 30	20 × 20	13
CWB (final)	20	30 × 30	25 × 25	21

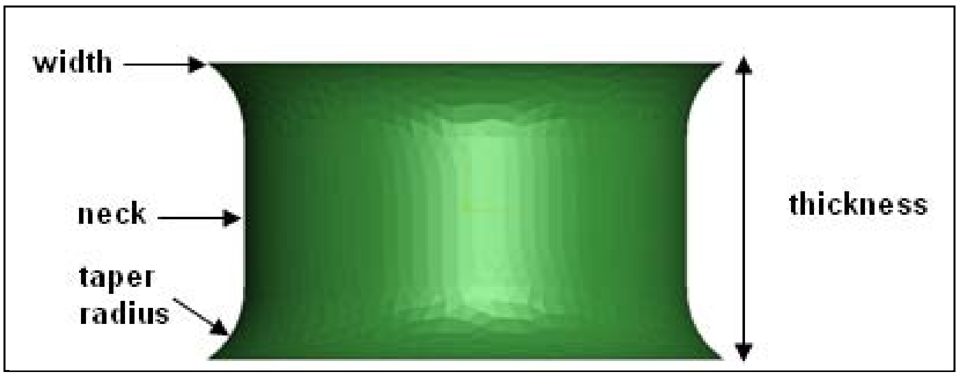

Figure 3. Schematic to illustrate iteration of specimen dimensions (actual appearance varies by specimen type).

Based upon the modeling results in table 2, the final geometry of the tapered cylinder and CWB specimens were selected for fabrication and testing. As per table 2, the RARDE-based specimen was deemed to have an unsuitable level of stress concentration and nonuniformity.

4. Experimental Methods

Tensile tests have been performed to evaluate the performance of the specimens selected after completion of modeling. At present, five repeats of each of the two final specimen types (figure 4a and b) have been performed to provide some measure of repeatability. Tests are performed on a hydraulic MTS* machine with a crosshead-mounted load cell. Full-field strain measurements are obtained via the digital image correlation (DIC) optical measurement

* MTS is a registered trademark of MTS Systems Corporation, Eden Prarie, USA.

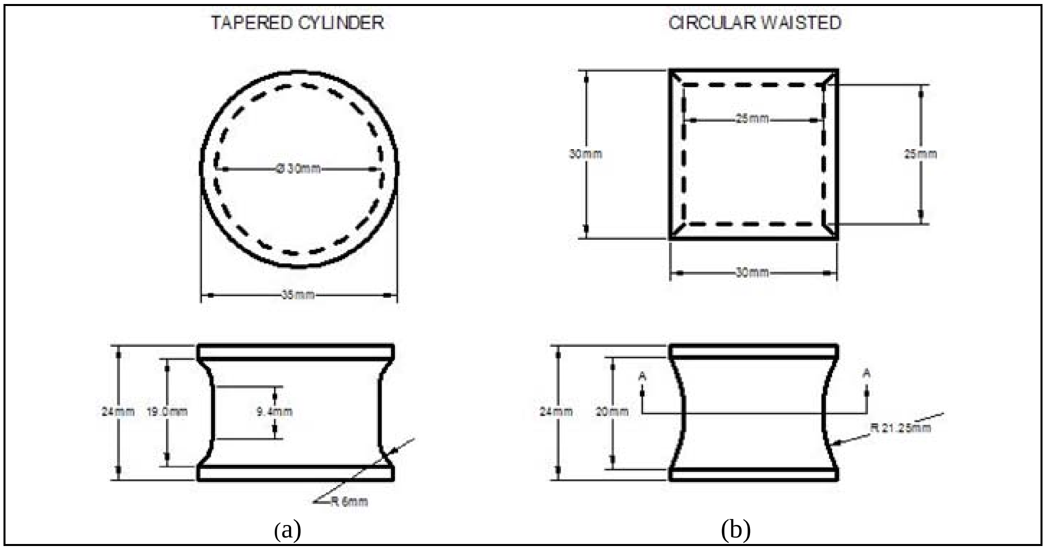

Figure 4. Specimens and dimensions chosen for testing: (a) tapered cylinder and (b) CWB.

technique. In this technique, a random speckle pattern is applied to the gauge section of the specimen. A pair of digital cameras then records a series of stereo images to track changes in the speckle pattern during testing. The images are post-processed with image correlation software (*16*), which tracks the relative displacement of all speckles within the pattern and computes 3-D surface strains from these displacements.

For comparison, strain gages were also applied but proved to be ineffective in maintaining adherence to the specimen for any appreciable strain level, especially for the large gage-section curvature of the CWB specimen. Using strain gages was also considered less desirable in that the strain response across the specimen is quite nonuniform. This strain field is measured completely by the full-field DIC measurements, whereas strain gages are limited to averaging across a given gage area. The DIC system also provides full motion video with superimposition of the real-time strain field. The magnified video images from the camera system also provide for excellent visualization and characterization of failure modes.

As a method of mounting each specimen to a test fixture, adhesive bonding of some trial specimens proved to be ineffective. The bond strength cannot be designed to be high enough with respect to the gage-section strength, given the minimum thickness needed to capture an adequate number of stitches across the cross section. An aluminum clamping fixture was designed to fit around the top and bottom shoulder of each specimen.

5. Experimental Results

Table 4 summarizes the results of uniaxial tension testing for the two specimen types of figure 4. A third column displays an adjusted value for the CWB test results, which are calibrated to account for the known stress concentration as determined from the modeling results (table 2).

Table 4. Average strength and stiffness properties from experimental testing of through-thickness specimens.

Geometry	Tapered Cylinder	CWB	CWB (Adjusted)
Experimental stiffness (GPa)	8.76	11.3	10.3
Standard deviation (%)	11.8	4.89	4.95
Difference from model stiffness prediction (%)	–5.19	21.9	11.3
Experimental strength (MPa)	20.9	27.9	25.4
Standard deviation (%)	22.8	17.6	17.6

This accounts for the fact that gage-section stresses will be higher than what is calculated from the applied load and cross-sectional area. Both the directly measured values and adjusted values are reported in table 4. Table 4 shows no comparison to modeling strength predictions, as the experiments are intended to establish the modeling capability for prediction of this failure mode.

The standard deviation on strength properties may seem quite high with reported values of 22.8% and 17.6%, but it should be noted that previous testing of in-plane properties consistently showed standard deviations on the order of 15% using well-known, consistent, standard techniques and specimens. A certain amount of inconsistency is inherent to the 3-D orthogonal architecture, given its nonhomogeneity, and microstructural complexity, which is given to manufacturing variability.

The tapered cylinder specimens had considerable issues with shoulder slippage through the clamping mechanism. This led directly to a lower measurement of peak load as the shoulder would begin to fail and decrease the specimen load capacity. This was seen only minimally in the CWB specimens, which exhibited more consistent results and a more reliable failure through the gage area.

The observed failure mode in all cases was initially pullout of the stitches, which separate from the bulk matrix after interfacial failure. This is followed by further interfacial failure as the warp and weft tows begin to separate. There is no fiber breakage or intertow matrix cracking, which are the typical failure modes for in-plane loading of the 3-D orthogonal architecture. As a consequence of the interfacial failure modes, the failure stress under uniaxial normal loading is relatively low (i.e., interfacial strength is relatively low compared to fiber strength). Failure was generally linear up to the peak load, with minor stiffness losses as stitches begin to debond. Past the peak load, fiber tows have begun to separate and peel off, and the specimen will continue to displace at a continually lower load. Thus the material is largely beyond its useful life, although this mechanical behavior does represent some continued energy absorption. Figure 5 presents an image captured from the DIC system with some salient features labeled. The nonuniformity of the strain field is readily apparent. The four stitches captured in this image are clearly shown to have pulled out of the surrounding material. Further, a zone of tow interface failure is seen, which causes a high strain region along the crack length.

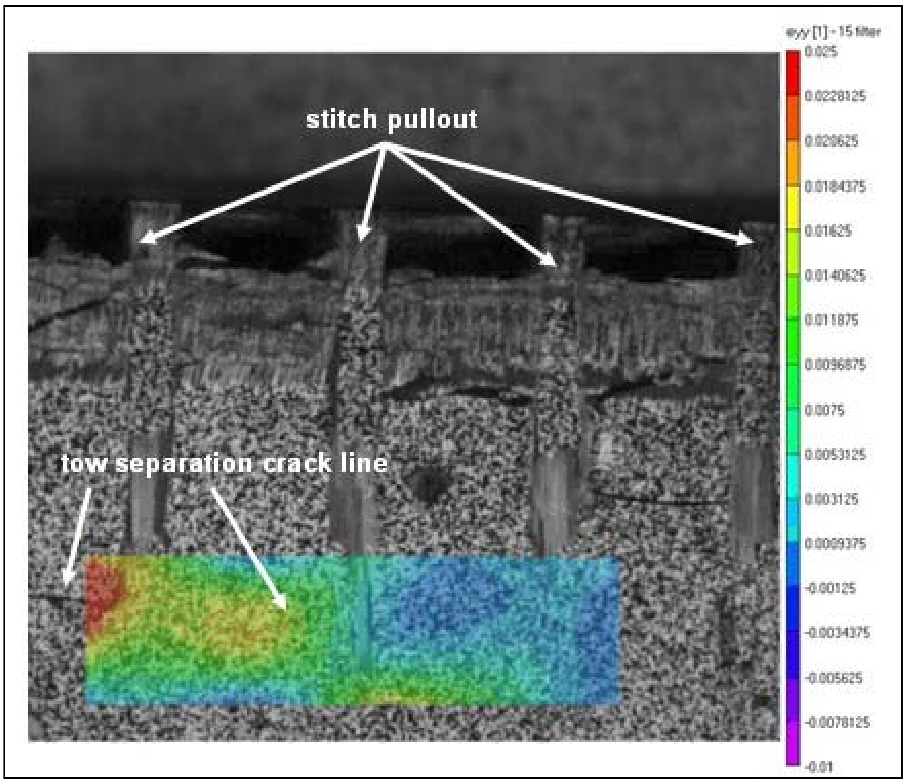

Figure 5. Direct video feed and strain field overlay from DIC system (width of view is ~14 mm; DIC strain contours will not be visible in black and white).

6. Conclusions

Tensile test specimens have been designed to provide direct measurement of through-thickness properties of a 3-D orthogonal-woven glass-epoxy composite, within the constraints of manufacturing feasibility and representation of the complex fiber microarchitecture. FEM modeling has been performed to evaluate multiple candidate specimens and determine their optimum geometry. Based on these results, two selected specimen types were fabricated and investigated experimentally. The observed failure mode was initially interfacial failure and pullout of the fiber stitches, followed by further interfacial failure as the warp and weft tows begin to separate. The specimens have shown good agreement with stiffness predictions as well as promising, consistent results for strength determination. Knowledge of these through-thickness properties provides direct improvement to material modeling capabilities and component design. Determining and characterizing the stitch-pullout and tow-separation failure modes under through-thickness loading allow for consideration of these failure modes and strength limits. Results show promising material capabilities, which can now be more easily understood and included in future designs and applications, including those requiring increased delamination resistance such as an insulator material for the electromagnetic railgun, or for thick composite parts or similar applications.

7. References

1. Callus, P. J.; Mouritz, A. P.; Bannister, M. K.; Leong, K. H. Tensile Properties and Failure Mechanisms of 3D Woven GRP Composites. *Composites: Part A* **1999**, *30*, 1277–1287.

2. Baucom, J. N.; Zikry, M. A. Evolution of Failure Mechanisms in 2D and 3D Woven Composite Systems Under Quasi-Static Perforation. *J. Comp. Mat.* **2003**, *37* (18), 1651–1674.

3. Takeshi, T.; Susuki, I. In-Plane and Out-of-Plane Characteristics of Three-Dimensional Textile Composites. *J. Comp. Mat.* **2005**, *39* (6), 543–556.

4. Baucom, J. N.; Zikry, M. A.; Rajendran, A. M. Low-Velocity Impact Damage Accumulation in Woven S2-Glass Composite Systems. *Compos. Sci. Technol.* **2006**, *66*, 1229–1238.

5. Yang, B.; Kozey, V.; Adanur, S.; Kumar, S. Bending, Compression, and Shear Behavior of Woven Glass Fiber-Epoxy Composites. *Composites: Part B* **2000**, *31*, 715–721.

6. Tarnopol'skii, Y. M.; Kulakov, V. L.; Aranautov, A. K. Measurements of Shear Characteristics of Textile Composites. *Composites and Structures* **2000**, *76*, 115–123.

7. Karkkainen, R. L.; Sankar, B. V. A Direct Micromechanics Method for Failure Initiation of Plain Weave Textile Composites. *Compos. Sci. Technol.* **2006**, *66*, 137–150.

8. Karkkainen, R. L.; Sankar, B. V.; Tzeng, J. T. A Direct Micromechanical Approach Toward the Development of Quadratic Stress Gradient Failure Criteria for Textile Composites. *J. Comp. Mat.*, in press.

9. Karkkainen, R. L.; Sankar, B. V.; Tzeng, J. T. Strength Prediction of Multi-Layer Plain Weave Textile Composites Using the Direct Micromechanics Method. *Composites Part B: Engineering*, in press.

10. Schubel, P. M.; Luo, J. J.; Daniel, I. M. Through-Thickness Characterization of Thick Composite Laminates. *Proceedings of the Society for Experimental Mechanics 2006 Annual Conference*, St. Louis, MO, June 2006.

11. Daniel, I. M.; Ishai, O. *Engineering Mechanics of Composite Materials*, 2nd ed.; Oxford University Press: New York, 2005.

12. Lodeiro, M. J.; Broughton, W. R.; Sims, G. D. Understanding the Limitations of Through-Thickness Test Methods. *Plastics, Rubber and Composites* **1999**, *28* (9), 416–424.

13. Broughton, W. R.; Gower, M. R. L. Through-Thickness Testing of Polymer Matrix Composites, material note MATC(MN)06, National Physical Laboratory, Middlesex, UK, May 2001.

14. Broughton, W. R.; Sims, G. D. *An Overview of Through-Thickness Test Methods for Polymer Matrix Composites;* NPL Report DMM(A) 148; National Physical Laboratory: Middlesex, UK, 1994.

15. Hodgkinson, J. M. *Mechanical Testing of Advanced Fibre Composites*; Woodhead Publishing Limited: Cambridge, UK, 2000.

16. Correlated Solutions, Inc. *VIC-3D User's Manual*; West Columbia, SC, 2005.

NO. OF COPIES	ORGANIZATION
1 (PDF only)	DEFENSE TECHNICAL INFORMATION CTR DTIC OCA 8725 JOHN J KINGMAN RD STE 0944 FORT BELVOIR VA 22060-6218
1	DIRECTOR US ARMY RESEARCH LAB IMNE ALC HRR 2800 POWDER MILL RD ADELPHI MD 20783-1197
1	DIRECTOR US ARMY RESEARCH LAB AMSRD ARL CI OK TL 2800 POWDER MILL RD ADELPHI MD 20783-1197
1	DIRECTOR US ARMY RESEARCH LAB AMSRD ARL CI OK PE 2800 POWDER MILL RD ADELPHI MD 20783-1197
	ABERDEEN PROVING GROUND
1	DIR USARL AMSRD ARL CI OK TP (BLDG 4600)

NO. OF COPIES	ORGANIZATION
1	DIRECTOR US ARMY RSRCH LAB AMSRD ARL SE DE R ATKINSON 2800 POWDER MILL RD ADELPHI MD 20783-1197
7	DIRECTOR US ARMY RSRCH LAB AMSRD ARL WM MB A ABRAHAMIAN M BERMAN M CHOWDHURY A FRYDMAN R KARGUS T LI T PLAISTED 2800 POWDER MILL RD ADELPHI MD 20783-1197
1	COMMANDER US ARMY TACOM ARDEC AMSTA AR WEA D KAPOOR BLDG 25 PICATINNY ARSENAL NJ 07806-5000
1	COMMANDER US ARMY TACOM ARDEC AMSRD AR AEMI S KERWIEN BLDG 61 N PICATINNY ARSENAL NJ 07806-5000
1	US ARMY TARDEC AMSRD TAR R D TEMPLETON 6501 E 11 MILE RD MS 263 WARREN MI 48397-5000
3	BENET LABS AMSTA AR CCB E KATHE A LITTLEFIELD P COTE WATERVLIET NY 12189

NO. OF COPIES	ORGANIZATION
4	US ARMY RSRCH OFC A CROWSON D MANN J PRATER B LAMATTINA PO BOX 12211 RSRCH TRIANGLE PARK NC 27709-2211
1	OFC OF NAVAL RSRCH J CHRISTODOULOU ONR CODE 332 800 N QUINCY ST ARLINGTON VA 22217-5600
4	NAVAL SURFACE WARFARE CTR CODE G33 K LEWIS D BRUNSON C GARNETT B MCGLASSON G32 DAHLGREN VA 22448
1	DARPA B WILCOX 3701 N FAIRFAX DR ARLINGTON VA 22203-1714
2	DIR LLNL STEVE DETERESA L-154 MILTON FINGER L-020 PO BOX 808 LIVERMORE CA 94550
3	NASA LANGLEY RSCH CTR AMSRD ARL VT F BARTLETT JR W JACKSON K O’BRIEN MS 266 HAMPTON VA 23681-0001
2	DARPA S WAX L CHRISTODOULOU 3701 N FAIRFAX DR ARLINGTON VA 22203-1714
3	INST FOR ADVANCD TECH H FAIR I MCNAB S BLESS 3925 W BRAKER LN AUSTIN TX 78759-5316

NO. OF COPIES	ORGANIZATION
1	ARMTEC DEFENSE PRODUCTS S DYER 85 901 AVE 53 PO BOX 848 COACHELLA CA 92236
2	PACIFIC NORTHWEST LAB G VAN ARSDALE R SHIPPELL PO BOX 999 RICHLAND WA 99352
1	CUSTOM ANALYTICAL ENG SYS INC A ALEXANDER 13000 TENSOR LANE NE FLINTSTONE MD 21530
2	GENERAL DYNAMICS OTS FLINCHBAUGH DIV K LINDE G KURZIK PO BOX 127 RED LION PA 17356
3	UNIV OF DELAWARE CTR OF COMPOSITE MTRLS J GILLESPIE S YARLAGADDA S ADVANI 215 COMPOSITES MANUFAC SCI LAB NEWARK DE 19716
1	UNIV OF DELAWARE CTR OF COMPOSITE MTRLS M SANTARE 126 SPENCER LAB NEWARK DE 19716
1	PENN STATE UNIV C BAKIS 212 EARTH ENGR SCIENCES BLDG UNIVERSITY PARK PA 16802

ABERDEEN PROVING GROUND

NO. OF COPIES	ORGANIZATION
1	US ARMY ATC CSTE DTC AT AD I W FRAZER 400 COLLERAN RD APG MD 21005-5059
38	DIR USARL AMSRD ARL CI AMSRD ARL DPT T MULKERN AMSRD ARL O AP EG FI M ADAMSON AMSRD ARL WM L BURTON J SMITH S KARNA J MCCAULEY P PLOSTINS T WRIGHT AMSRD ARL WM B M ZOLTOSKI J NEWILL AMSRD ARL WM M S MCKNIGHT J BEATTY R DOWDING H MAUPIN AMSRD ARL WM MA M VANLANDINGHAM AMSRD ARL WM MB J BENDER T BOGETTI R CARTER W DE ROSSET W DRYSDALE R EMERSON D HOPKINS R KASTE L KECSKES E KLIER M MINNICINO B POWERS D SNOHA J SOUTH J SWAB J TZENG AMSRD ARL WM MC M MAHER AMSRD ARL WM MD E CHIN B CHEESEMAN C YEN AMSRD ARL WM T P BAKER AMSRD ARL WM TA C HOPPEL